

Behavior of grouped stud shear connectors between precast high-strength concrete slabs and steel beams

Zhuangcheng Fang, Haibo Jiang*, Gongfa Chen, Xiaotong Dong and Tengfei Shao

School of Civil and Transportation Engineering, Guangdong Univ. of Technology,
Guangzhou Higher Education Mega Center, Guangzhou, 510006, China

(Received May 15, 2019, Revised February 14, 2020, Accepted February 17, 2020)

Abstract. This study aims to examine the interface shear behavior between precast high-strength concrete slabs with pockets and steel beam to achieve accelerated bridge construction (ABC). Twenty-six push-out specimens, with different stud height, stud diameter, stud arrangement, deck thickness, the infilling concrete strength in shear pocket (different types of concrete), steel fiber volume of the infilling concrete in shear pocket concrete and casting method, were tested in this investigation. Based on the experimental results, this study suggests that the larger stud diameter and higher strength concrete promoted the shear capacity and stiffness but with the losing of ductility. The addition of steel fiber in pocket concrete would promote the ductility effectively, but without apparent improvement of bearing capacity or even declining the initial stiffness of specimens. It can also be confirmed that the precast steel-concrete composite structure can be adopted in practice engineering, with an acceptable ductility (6.74 mm) and minor decline of stiffness (4.93%) and shear capacity (0.98%). Due to the inapplicability of current design provision, a more accurate model was proposed, which can be used for predicting the interface shear capacity well for specimens with wide ranges of the stud diameters (from 13 mm to 30 mm) and the concrete strength (from 26 MPa to 200 MPa).

Keywords: push-out test; steel-precast slabs; grouped studs shear connector; high-strength concrete; accelerated bridge construction

1. Introduction

Steel-concrete composite beams, which combine the advantages of both materials, have been widely applied in infrastructure and bridge engineering in the last decades (Kim *et al.* 2011, Xu and Sugiura 2014). Conventional construction of steel-concrete composites, however, often require a lot of time due to in-situ concrete slab casting for temporary supports and formwork (Pavlović *et al.* 2013). For accelerated construction, an economical precast concrete deck system, as depicted in Fig. 1, has been used in several countries (Shim *et al.* 2001). Compared with traditional steel-concrete composite structure, this superior one has several advantages, such as minimizing on-site construction time and alleviating traffic impediment for bridge engineering, improving the safety and long-term performance of constructions, becoming both eco-friendly and economical because of the removing of framework and reducing of work in place, and so on (Noel *et al.* 2016, Lam 2008). It is the shear connector, in the narrow shear pocket, that enables the shear force transferred along the interface between the prefabricated concrete decks and steel girders and limits the separation/uplift between these two members, and that ensures the composite action (Lam 2008). After the failure of shear connectors, the composite action of composite structure decreases, causing a significant

reduction of stiffness (Fang *et al.* 2018).

The shear connector, as a crucial element, enhances the longitudinal shear capacity and prevents the separation in precast deck composite system (Ju and Zeng 2015). Several sorts of shear connectors have been proposed and used in composite structures, e.g., head stud (Shim *et al.* 2004, Su *et al.* 2014, Cao *et al.* 2017), perfobond (Machacek and Studnicka 2002, Zheng *et al.* 2016b, Wang *et al.* 2018b), bolts (Liu *et al.* 2015, Milosavljevic *et al.* 2018, Yang *et al.* 2018), crestbond (Classen and Hegger 2017, Chu *et al.* 2016), channel (Shariati *et al.* 2012, Fanaie *et al.* 2015, Paknahad *et al.* 2018), Y/I shaped (Kim *et al.* 2013, Mazoz *et al.* 2013, Kim *et al.* 2019), etc. However, most have various limitations in manufacture, assembling or even the structural performance. Comparatively, the head stud connectors, developed by Nelson Welding Company in 1940s, have been the most adopted shear connectors due to their economical and constructional advantages (Xu and Sugiura 2013). The mechanical behavior of connectors, especially for head stud connectors, was determined by the commonly used push-out tests suggested in Euro.4 (Eurocode 2005). From the standard push-out test for head stud shear connectors, three failure modes could be observed, that is, full yield of head studs without any concrete failure, concrete cone crushing with no stud shearing off, and the combination of stud shearing off and concrete crushing. These failure modes, closely related to the shear strength and load-deformation relationship of head

*Corresponding author, Professor
E-mail: hbjiang@gdut.edu.cn

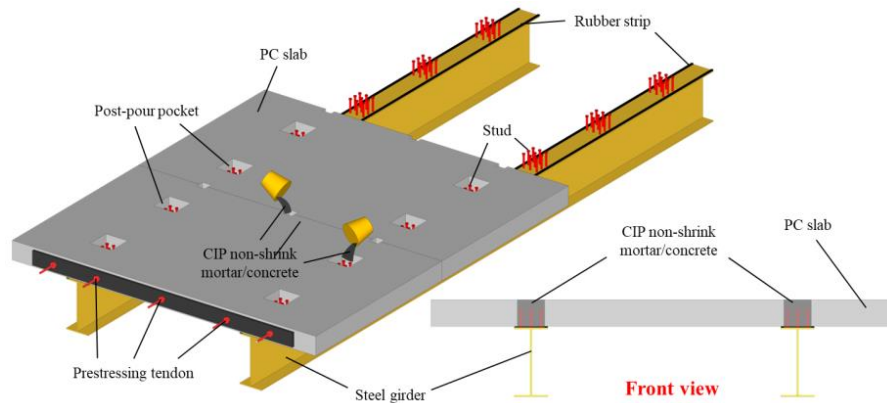


Fig. 1 Schematic diagram of prefabricated steel-concrete composite deck system

stud connectors, dependent on the sizes and material properties of studs (Lam and El-Lobody 2005, Zhu *et al.* 2013), the elastic modulus and compressive strength of the concrete (Lee *et al.* 2014, Kim *et al.* 2015, Xu *et al.* 2017a), concrete casting process (Wang *et al.* 2018a) and arrangement or the welding quality of studs (Wang *et al.* 2018a, Qi *et al.* 2017, Xu *et al.* 2012). Due to the losing of continuity for shear connectors, arranging studs in groups at the narrow shear pocket may be a useful method to improve the horizontal shear capacity of precast steel-concrete composite deck system (Xu and Sugiura 2013). In this case of grouped stud shear connectors, however, were on a complicated stress status, due to load concentration and combination of longitudinal shear and transverse bending actions, which causes the unfavorable shear stiffness reduction, shear strength degradation and interlayer splitting (Shim *et al.* 2001, Xu *et al.* 2012). In order to extend the current design codes to cover the shear connection in such a precast girder system, it is necessary to conduct lots of experimental tests and propose empirical equations based on the tests. So far, a few relevant studies have been reported. Based on these limited studies, it can be found that both failure modes and shear capacity of test specimens were highly dependent on the properties of the shear connectors, the infilling material and prefabricate concrete slab, but insensitive to the reinforcement arrangement in both the shear pocket and concrete deck (Wang *et al.* 2018a, Xu *et al.* 2012, Pavlović *et al.* 2013).

Despite the above mentioned studies on the behavior of precast deck systems, most of them utilized normal strength concrete to conduct the precast slab or used normal strength concrete/mortar as the pocket infilling materials. On the other hand, the diameter of studs in these studies were smaller than 16 mm, which may be widely adopted in structural engineering but not bridge engineering. For bridge engineering, diameter ranged from 19 mm to 25 mm may be suitable to ensure the whole structural performance. Considering the actual needing in bridge engineering, this size of studs may also be more economical and effective. At the same time, prefabricated high-strength concrete slab and higher strength pocket infilling concrete/mortar should also be chosen in this system to make full utilization of the material properties. However, related investigations on the static behavior of grouped studs embedded in the precast

high-strength concrete slab were very limited.

In this paper, 26 push-out tests were carried out to investigate the mechanical behavior of precast high-strength deck system with grouped head studs in the pocket. Beside the shear behavior, this study also aims at understanding the effects of the stud height and diameter, deck thickness, cast-in-place concrete strength/different types of concrete, steel fiber volume in the shear pocket concrete, casting method and the arrangement of stud to further explore the applicability of this composite structure. Based on the test results and previous studies, the shear bearing capacity, shear stiffness and shear-slip behavior of grouped stud shear connectors in precast high-strength concrete slab with pockets were comprehensively evaluated. The applicability of current design codes was also examined and then a more accurate model was proposed. Additionally, the work presented in this paper fills a current knowledge gap that has not been addressed by previous studies about the behavior of grouped stud shear connectors between precast high-strength concrete slabs and steel beams. On the other hand, the founding here was more suitable for introducing the prefabricated steel-concrete composite deck system to the field of accelerated bridge construction.

2. Experimental program

2.1 Test specimens

The experimental program was consisted of twenty-six push-out tests, twenty-four of which utilized pocket slab and the remaining used monolithic cast slab. The configurations of the specimens are shown in Fig. 2, which is similar to the recommendation in the Eurocode 4 (Eurocode 2005). The dimensions of the concrete slab were 650 mm × 600 mm × 250 mm and those of the pocket were 225 mm × 225 mm × 250 mm. In the concrete slab, rectangular steel reinforcements were placed in both longitudinal and transverse directions to prevent unexpected failures. A cover thickness of 15 mm was chosen for all specimens. To represent the steel component in composite members, a 650-mm-height H-shaped steel beam with a cross section of 300 mm × 300 mm × 15 mm × 10 mm was selected. Specially, the spacing between the stud shear

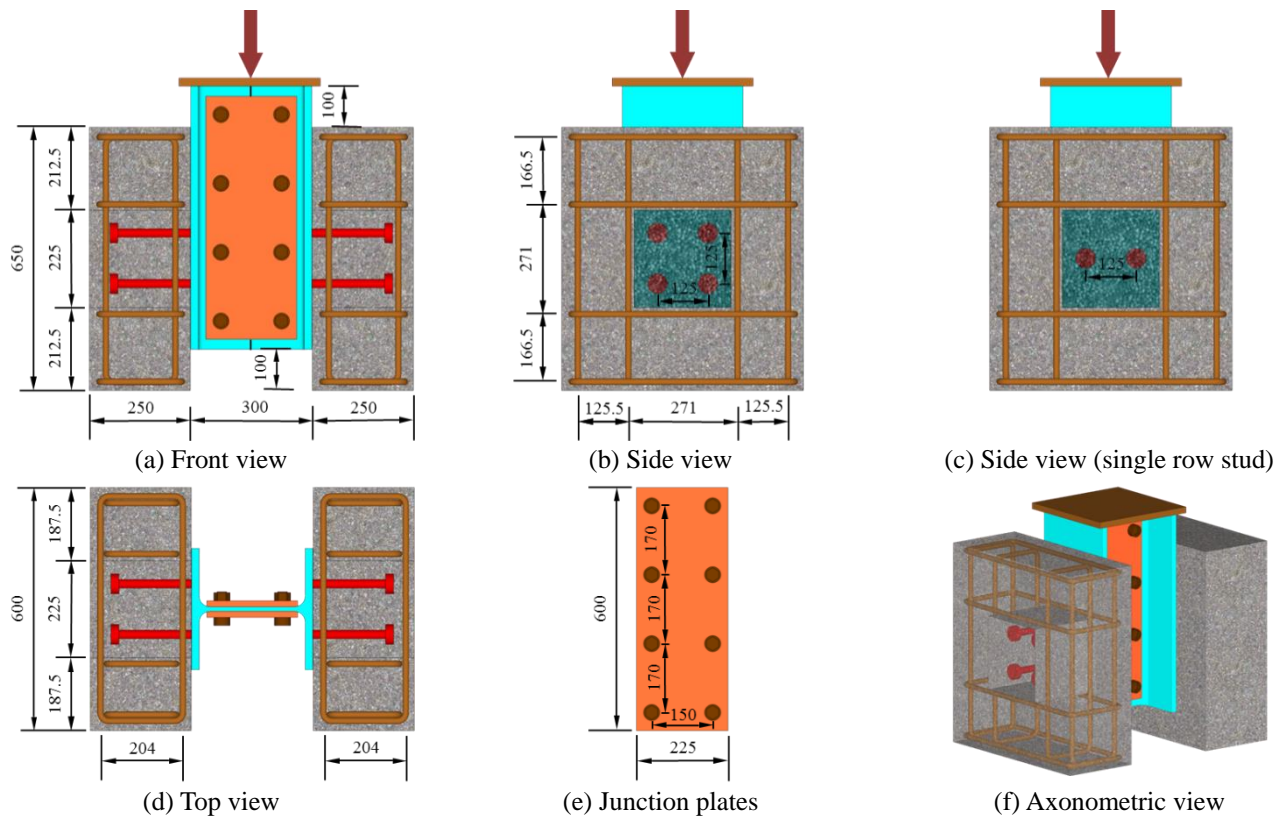
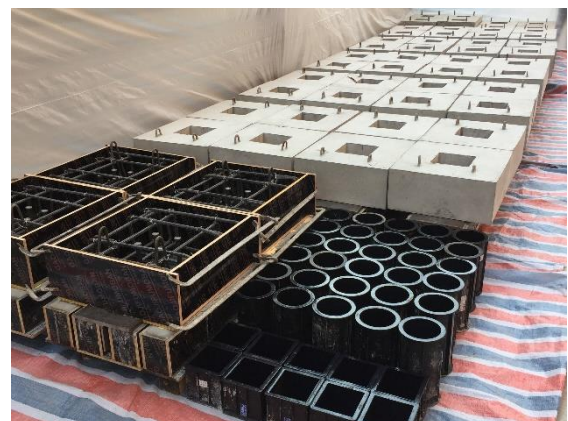


Fig. 2 Configurations of push-out specimens



(a) Formwork of precast slab



(b) Casting of pocketed concrete

Fig. 3 Fabrication procedure of test specimens

connectors in the pockets was 125 mm in both vertical and horizontal direction, which met the requirement in Eurocode 4 (Eurocode 2005) for the minimum spacing of $5d$ in all cases. Additionally, two duplicates for each type of specimens were conducted to consider the deviations due to material difference, testing instrumentation or manufacturing errors.

The fabrication procedure of tested specimens is shown in Fig. 3. The concrete slabs with a pocket were cast first to simulate a precast flange in a horizontal position, as is done in engineering practice (Fig. 3a). After curing in moist condition for two weeks, the precast concrete slabs were placed on the steel beam at horizontal direction (Fig. 3(b)),

which was the same as the process of actual engineering and ensured the quality of the pocket concrete. Thus, the steel component of specimen was divided into two T-shaped beams, which were assembled with bolts until the testing day. Bonding at the interface between steel beam and the concrete slab had been prevented by greasing the steel flange, as required in Eurocode 4 (Eurocode 2005). It can be noted that the monolithic specimens were cast at the same time of cast-in-place (CIP) pocket concrete. After two weeks of moist condition curing, these specimens were left outside the laboratory for natural curing until placed in the testing machine. All the control cylinders were cured under the same condition as the corresponding specimens.

Table 1 Series designation and test matrix

Specimen	Stud height h (mm)	Stud diameter d (mm)	Aspect ratio	Slab thickness T (mm)	Pocket concrete strength (MPa)	Volume of steel fiber v
200/19-250-C85-0	200	19	10.53	250	85 (C85)	0
200/22-250-C85-0	200	22	9.09	250	85 (C85)	0
200/25-250-C85-0	200	25	8.00	250	85 (C85)	0
150/22-250-C85-0	150	22	6.82	250	85 (C85)	0
100/22-250-C85-0	100	22	4.54	250	85 (C85)	0
150/22-200-C85-0	150	22	6.82	200	85 (C85)	0
150/22-300-C85-0	150	22	6.82	300	85 (C85)	0
200/22-250-C100-0	200	22	9.09	250	100 (C100)	0
200/22-250-R125-0	200	22	9.09	250	125 (R125)	0
200/22-250-MC85-0	200	22	9.09	250	85 (C85)	0
200/22-250-C85-1	200	22	9.09	250	85 (C85)	1%
200/22-250-C85-2	200	22	9.09	250	85 (C85)	2%
S200/22-250-C85-0	200	22	9.09	250	85 (C85)	0

2.2 Parameters

Five primary variables were investigated in this study, including the height and diameter of studs, the slab thickness, the compressive strength of pocket concrete, and the volume of steel fiber. As a reference, a monolithically cast specimen and a single-row stud were conducted. As summarized in Table 1, the height of studs varied from 100 mm to 200 mm, while the diameter of studs varied from 19 mm to 25 mm. With the combining of different stud heights and stud diameters, the aspect ratio ranged from 4.54 to 10.53. The thicknesses of precast concrete slabs were set as 200, 250 and 300 mm to investigate its influence. Specimens were constructed with high-strength concrete with target f_c' of 85 MPa (f_c' is the measuring cylinder concrete strength at test day), high-strength concrete with expected f_c' of 100 MPa, and reactive powder concrete (RPC) with f_c' of 125 MPa in the pocket. In order to study the effect of steel fiber volume in pocket concrete, both 1% (75 kg/m³) and 2% (150 kg/m³) volume ratio of steel fiber were considered.

2.3 Material properties

Six different concrete mixes with water-cement ratio ranging from 0.29 to 0.40 were used to fabricate the testing specimens, including one type for precast/monolithic slab and five types for CIP pockets. Details of each concrete mixture proportion and other properties of concrete mixtures are listed in Table 2, including the compressive strength of concrete at test day f_c' (ASTM 2015), splitting tensile strength f_t (ASTM 2011), elastic modulus E_c (ASTM 2014), and Poisson ratio (ASTM 2014). All the properties were determined using the standard cylinders, which were cured under the same condition as the corresponding test specimens. It can be noted that all the precast concrete slabs were fabricated with the same concrete. Specially, the concrete with both 1% and 2%

volume ratio of steel fiber for the pocket, had a measured compressive strength f_c' closed to that of C100 concrete.

All the headed studs used in this experiment were made from the same type of material, with the nominal yield strength f_y and ultimate strength f_u of 345 and 430 MPa, respectively. The actual yield strength and ultimate strength for headed studs with different diameters are also listed in Table 2. As mentioned previously, the steel beam sections were HW 300 × 300 in Q235B steel (nominal yield strength of 235 MPa), while the measured yield strength and ultimate strength were 253.29 and 425.03 MPa, respectively. Additionally, all the reinforcements in the precast concrete slab were made of 16-mm-diameter HRB 400 corrugated bars (nominal yield strength of 400 MPa), with the practical yield strength and ultimate strength of 431.61 MPa and 596.63 MPa, respectively.

2.4 Test setup and loading procedure

The test setup for this experiment is illustrated in Fig. 4. A hydraulic loading machine with a capacity of 10000 kN was used to conduct the push-out tests. As shown in the figure, four Linear Variable Differential Transformers (LVDTs) were employed to measure the longitudinal displacement between the precast concrete slab and the steel beam, while another four horizontal LVDTs were installed to record the relative uplift between them. These LVDTs were mounted on the same height level with the middle of shear pocket, which was 325 mm away from the bottom of the precast concrete slab.

A two-phase loading procedure followed the Eurocode 4 (Eurocode 2005) recommendation was employed for all the push-out tests in this study. At the first loading stage, the applied load cycled 25 times from 5% up to 40% of the expected failure load [calculated by Eq. (3)] in a rate of 10 kN/s. At this stage, the bonding between the steel beam and precast concrete slab had been broken. At the following phase, the specimens were tested up to failure at a speed of

Table 2 Materials properties

Type		PC slab concrete	CIP concrete (C85/MC85)	CIP concrete (1% SF)	CIP concrete (2% SF)	CIP concrete (C100)	CIP concrete (R125)	
Concrete	Coarse aggregate	1105	1050	1050	1050	1133	--	
	Sand	595	671	671	671	695	960	
	Cement	395	523	523	523	517	800	
	Mixture design quantities (kg/m ³)	Water	160	183	183	183	155	232
	Water reducer	10	--	--	--	4.5	25	
	Fly ash	105	--	--	--	--	--	
	Expansive agent	--	31.38	31.38	31.38	31.02	48	
	Steel fiber	--	--	75	150	--	150	
	Silica fume	--	--	--	--	--	240	
	f_c' at test day (MPa)		72.12	87.76	101.81	100.92	103.12	125.28
f_t (MPa)		4.98	5.71	7.56	10.06	6.79	12.14	
E_c (MPa)		35788	42345	43464	46467	43833	--	
Poisson's ratio		0.204	0.249	0.268	0.252	0.227	--	
Steel products	Type	ϕ 19 stud	ϕ 22 stud	ϕ 25 stud	Steel beam	Reinforcement		
	f_y (MPa)	342.40	358.15	335.49	253.29	431.61		
	f_u (MPa)	470.66	484.75	459.11	425.03	596.63		

* SF: Steel fiber

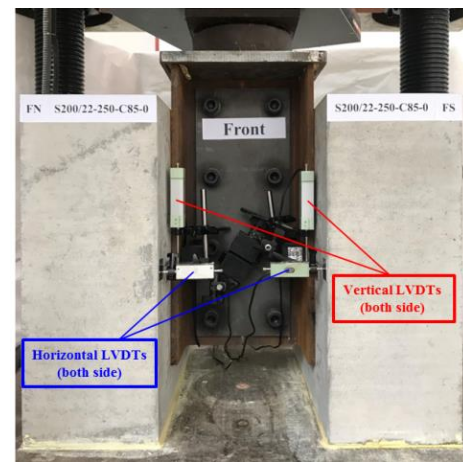


Fig. 4 Test setup for push-out tests

0.3 mm/min. The loading procedures were terminated when the interface shear capacity decreased to 50% of the ultimate load.

3. Test results and discussion

3.1 Observed Behaviour

The shear failure modes were similar for all the specimens, as depicted in Fig. 5. On the outer surfaces of the slab, several lateral cracks or cracks around the pockets were observed, as presented in Fig. 5a. Actually, the cracks were first formed around the flange of slab and then

developed or even crossed with each other in the middle of specimens. These lateral cracks were related to the out-of-plane bending moment M on concrete slab and will be discussed deeply in the next part. After reaching the ultimate load, no further cracking could be observed. This type of cracking pattern can also be seen from several specimens in this study. Particularly, no cracks were found on the surface of concrete slab for the tests with the thickest slab (150/22-300-C85-0), with single-row-stud (S200/22-250-C85-0) or the monolithically-cast ones (200/22-250-MC85-0).

On the inner surfaces of the slab, almost all of the shear connectors showed studs fracture near its roots, with the apparent crushing at adjacent concrete. Interesting, bending

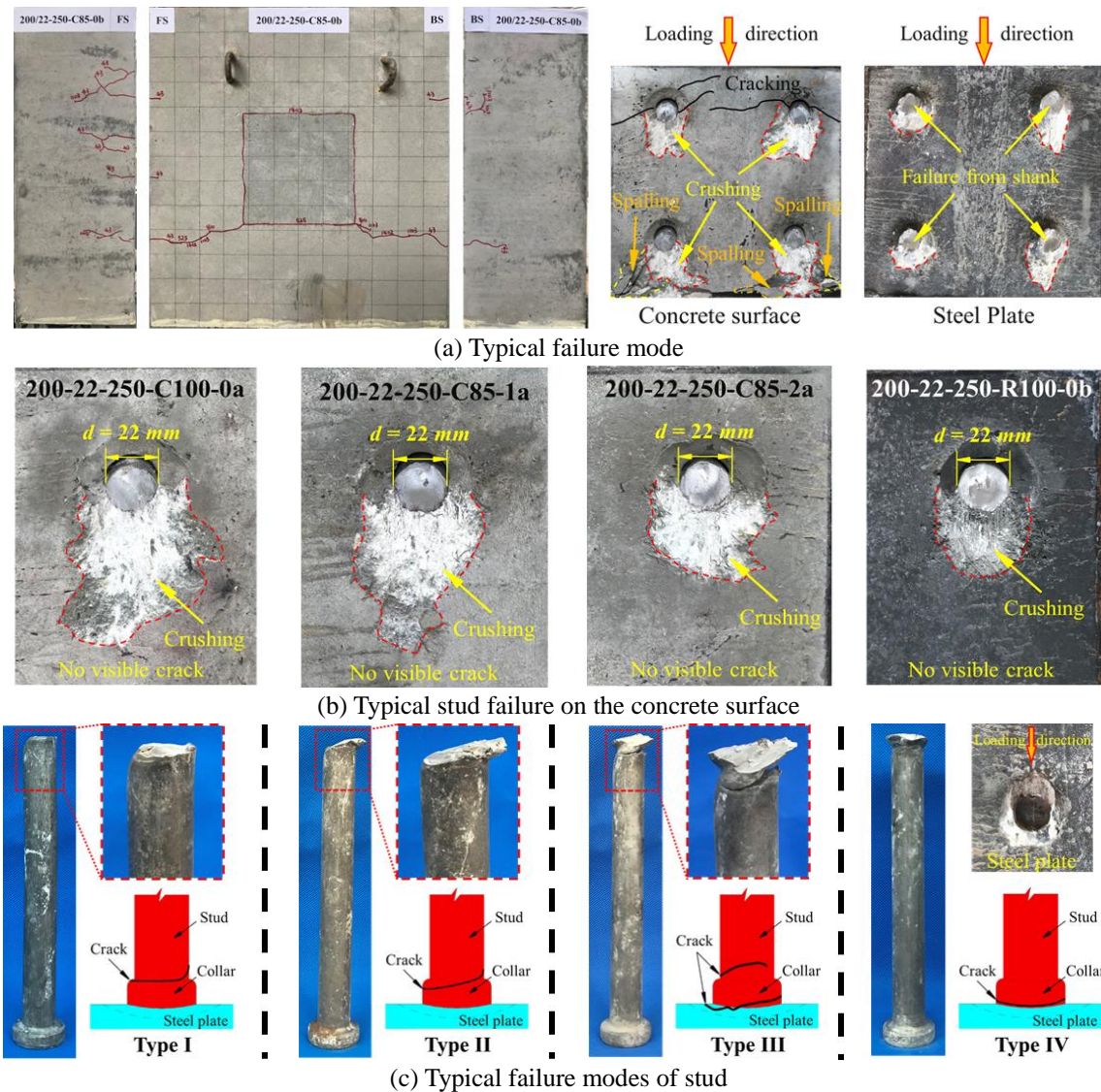


Fig. 5 Failure modes of specimens

cracks or diagonal cracks were noted around the upper studs, while spalling of concrete would only be found near the lower studs. However, this phenomenon can't be observed in specimens with high-strength pocket concrete (more than 100 MPa) or with steel fiber in pocket concrete, as displayed in Fig. 5(b). In these specimens, only the concrete crushing was displayed, without any visible cracks even at the end of the test, which indicated that the concrete strength of 100 MPa was high enough to bear the ultimate load in the tests and the fiber-bridge effect (Wang *et al.* 2018a) had limited the cracking efficient in these cases.

On the other hand, totally four types of stud failure modes had been recorded, as illustrated in Fig. 5(c). Type I mode showed perfect fracture of stud, which utilized the properties of shear stud sufficiently and occurred in most of the tests. Type II and Type III failure modes of stud presented unexpected results, with the crucial ruptured crack crossing both the stud and welding collar areas. This result may be associated with both the shear stress concentration at shank area of studs and the random failure of connectors. Luckily, the little deviation of shear behavior

demonstrated that the capacity of shear studs in these cases had not been cut down. However, the worst welding defects (Type II in Fig. 5(c)) had also been detected occasionally, which took place in the welding flaws zone at stud collar and was very harmful for the stud properties (Shim *et al.* 2004, Xu *et al.* 2012, Han *et al.* 2015). This welding defect decreased the bearing capacity directly when it occurred before reaching peak load (Specimen S200/22-250-C85-0b). While the ultimate shear loads would not be affected apparently, the ductility of studs may be incorrect as this type of failure happened at post-peak load stage (100/22-250-C85-0b). In order to draw a rational conclusion, the results of these two specimens were not adopted.

3.2 Applied shear-slip relationship

The load-slip curves for all specimens are plotted in Fig. 6. High similarity among the curves can be noticed, which may be generalized by the dotted curve as shown in Fig. 7. Three significant points, clearly distinguished by a rapid change in the slope, were marked as a, b, and c in Fig. 7.

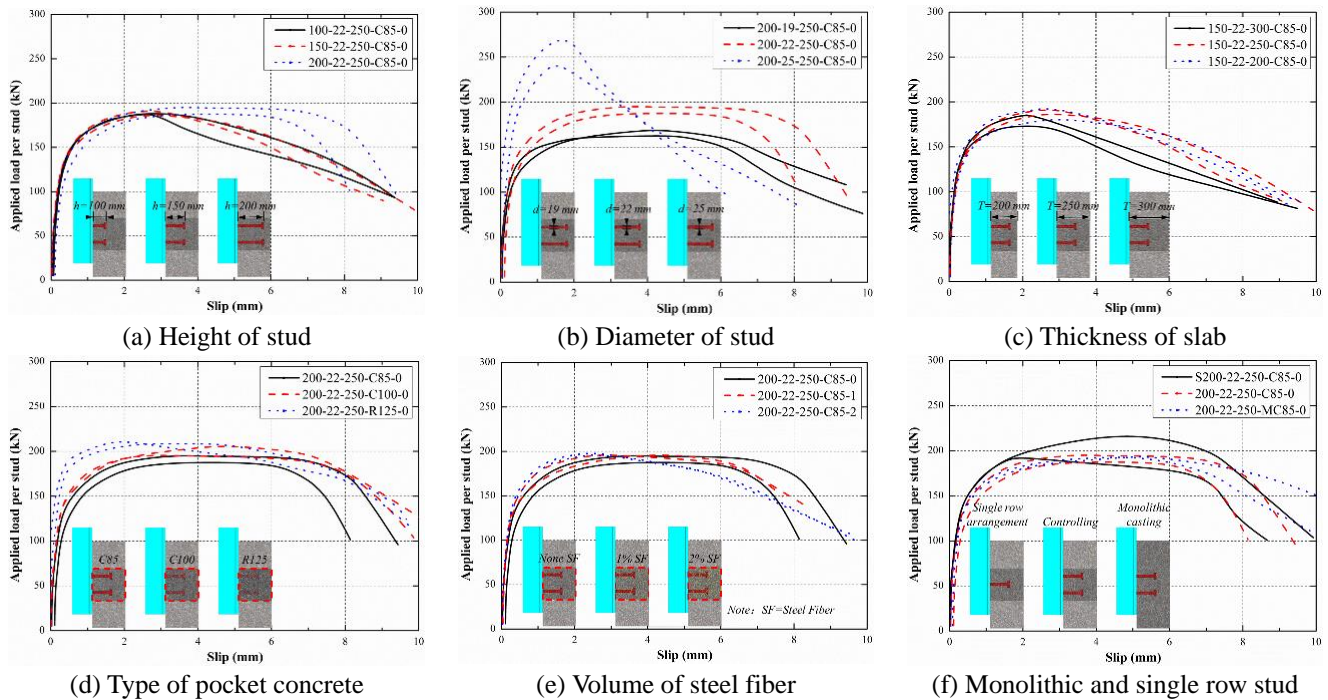


Fig. 6 Load-slip relationship

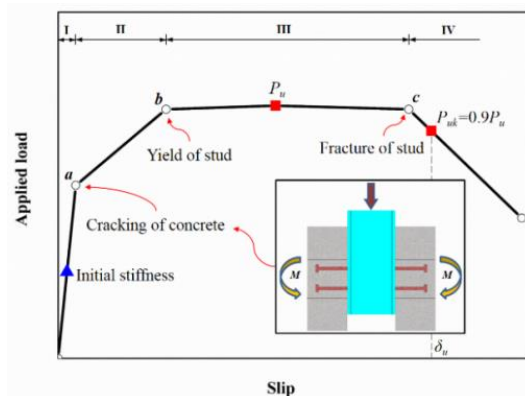


Fig. 7 Typical response in terms of slip under applied load

With loading, the steel beam began to slip, thus, as shown in the figure, an out-of-plane bending moment M was induced on the concrete slab. This bending action was produced by the uplift effect as a result of the separation between the steel girder and concrete slab (Xu *et al.* 2012). Once the tensile stress induced by M was larger than the ultimate tensile strength of concrete, cracks were then formed at the side of precast concrete slab (point a). At this stage, the rise of the curve slows down apparently and the cracks get longer and wider, accompanied with the monotonic ascending of both loads and slip. Due to the yielding of stud, the curve slope reduced and the capacity of specimens approached a reasonably horizontal level. At the third branch, any attempted to increase the shear capacity would then result in large slip and the maximum shear capacity was reached at this stage. At the end of this phase, fracture of head stud would happen, resulting in a drop in the applied load. The loss of head stud was marked as point c . Subsequently, more and more shear connectors failed,

causing the consistently decrease of load capacity.

Compared with the load-slip relationship in Fig. 6, it can be noted that most of the tests did not experience all four stages described above, especially the phase III. Similar behaviours can be noted in previous study (Li and Cederwall 1996, Han *et al.* 2015). This stage initiated at the yield of head stud, and terminated at the fracture of connectors. Since the non-uniform of shear stress existed on each stud, the one in the worst situation would fracture first. Once these two events occurred successively in a very short time interval, the effect of the phase III would not be clearly reflected (e.g. 200-25-250-C85-0, etc.). These may also be the reason for the phenomenon of abrupt load decrease soon after a peak load and the proposing of idealized tri-linear curve (Shim *et al.* 2004). Coincidentally, this type of load-slip relationship was presented in all the specimens with shorter studs (with the height of 150 mm or 100 mm), which showed that the height of shear connector made an apparent influence on its behaviour at post failure stage.

3.3 Initial stiffness

The initial stiffness for shear connectors, defined as the secant slope at the slip of 0.2 mm (Xu *et al.* 2014, Zheng *et al.* 2016a), are summarized in Table 3. As an indicator to reflect the deformation ability of studs, the initial stiffness was used to evaluate the performance of the bridge global behaviour in serviceability limit state (Wang *et al.* 2018a).

The initial phase of load-slip curves (Fig. 6) for specimens with stud height varying from 100 mm to 200 mm almost maintained almost the same slope, which indicated that the initial stiffness might be insensitive to the stud height. Identical concrete materials and stud diameters also proved that the anchorage length of 100 mm for stud

Table 3 Summary of test result

No.	Specimen	Stiffness (kN/mm)		Load capacity per stud				Slip capacity			
				P_u (kN)		P_{RK} (kN)		δ_u (mm)		δ_{uk} (mm)	
1	200/19-250-C85-0a	4179.32	4113.85	162.33	165.76	146.09	149.18	6.31	6.50	5.67	5.85
2	200/19-250-C85-0b	4048.37		169.19		152.27		6.69		6.02	
3	200/22-250-C85-0a	4251.39	4378.31	187.48	191.29	168.73	172.16	6.96	7.48	6.27	6.74
4	200/22-250-C85-0b	4505.22		195.10		175.59		8.01		7.20	
5	200/25-250-C85-0a	5929.10	5833.80	271.31	257.21	244.18	231.49	2.32	2.39	2.09	2.15
6	200/25-250-C85-0b	5738.49		243.11		218.80		2.46		2.21	
7	150/22-250-C85-0a	4632.90	4597.24	192.05	189.76	172.84	170.79	4.58	5.07	4.12	4.57
8	150/22-250-C85-0b	4561.58		187.48		168.73		5.56		5.01	
9	100/22-250-C85-0a	4590.42	4590.42	188.24	188.24	169.42	169.42	5.33	5.33	4.80	4.80
10	100/22-250-C85-0b	4551.20	*	187.48	*	168.73	*	3.77	*	3.40	*
11	150/22-200-C85-0a	4682.20	4574.62	192.81	187.48	173.53	168.73	4.63	5.30	4.17	4.77
12	150/22-200-C85-0b	4467.03		182.14		163.93		5.96		5.36	
13	150/22-300-C85-0a	4984.19	4941.52	185.95	179.48	167.36	161.53	3.59	3.67	3.23	3.30
14	150/22-300-C85-0b	4898.86		173.00		155.70		3.74		3.37	
15	200/22-250-C100-0a	4964.25	4769.13	195.86	201.19	176.27	181.08	8.04	7.90	7.24	7.11
16	200/22-250-C100-0b	4574.02		206.53		185.88		7.76		6.99	
17	200/22-250-R125-0a	5604.98	5619.22	212.63	210.72	191.36	189.65	5.74	6.41	5.16	5.77
18	200/22-250-R125-0b	5633.46		208.82		187.93		7.09		6.38	
19	200/22-250-MC85-0a	4747.19	4605.30	192.81	193.19	173.53	173.87	7.30	7.90	6.57	7.11
20	200/22-250-MC85-0b	4463.42		193.57		174.22		8.50		7.65	
21	200/22-250-C85-1a	5149.80	4967.16	195.86	195.86	176.27	176.27	6.81	6.85	6.13	6.16
22	200/22-250-C85-1b	4784.52		195.86		176.27		6.89		6.20	
23	200/22-250-C85-2a	5120.75	4854.52	198.91	197.38	179.02	177.65	5.47	5.56	4.93	5.00
24	200/22-250-C85-2b	4588.30		195.86		176.27		5.64		5.07	
25	S200/22-250-C85-0a	2270.92	2270.92	217.96	217.96	196.17	196.17	7.27	7.27	6.55	6.55
26	S200/22-250-C85-0b	2408.25	*	193.57	*	174.22	*	6.55	*	5.89	*

* Test results have not been included to draw the conclusions due to its poor welding quality; δ_u : Denoted the displacement at the instant of peak load; δ_k : Denotes the displacement at the instant when the peak load decreases by 10%

with a diameter of 22 mm was sufficient. A slight influence on initial stiffness for the variable of slab thickness can be noticed, raising the thickness from 200 mm to 300 mm led to only 8.02% increase in the initial stiffness. This minor deviation showed that the increasing of slab heights would not make the stud shear connectors stiffer apparently.

The load-slip relationship curves shown in Fig. 6 also revealed that, for the same size of shear pocket, an increase in stud diameter made stage I stiffer. The stiffness of specimen with the 25 mm stud was 1.42 times that of the 19 mm stud. In another word, the larger the diameters of headed stud, the shear connectors have the better initial stiffness. With the same pocket concrete, stiffer larger headed studs reflected smaller deformations in the specimens, resulting to the higher stiffness of connectors.

The strength of shear pocket concrete also had apparent effects on the initial stiffness, as listed in Table 3. Compared with the C85 concrete, using C100 concrete or R125

concrete got 9% and 28% increase in stiffness, respectively. With addition of steel fiber in cast-in-place concrete, the stiffness of specimens had also been enhanced. Nevertheless, no much distinction could be observed between different volumes of steel fiber in shear pocket concrete. The initial slip of stud shear connectors in the early loading stage owed to surrounding concrete cracking and stud deformation (Kim *et al.* 2015). A large number of tensile cracks or concrete spalling around the studs also increased the slip of specimens (Wang *et al.* 2018a). With both the increasing of concrete strength or volume of steel fiber in post-pour concrete, a great improvement of tensile strength for the mixtures can be noted (Table 2). This change had limited the development of cracking around the slabs (Fig. 5), causing a higher stiffness of the corresponding tests. This founding also affirmed the result that thinner compressive zone of RPC was sufficient to transfer and balance the external load due to its higher

compressive strength (Wang *et al.* 2018a).

For monolithically cast specimens, only 5% increase of stiffness was found, which indicated that using precast concrete slab with shear pocket would also obtain a reasonable initial stiffness. The slight difference of stiffness between them may result from the deformation of shear pocket concrete, which has a lower restraint from the surrounding concrete. In another word, the initial stiffness of specimens depended on the properties of stud and adjacent concrete. Similar conclusion can also be drawn in the comparison of specimens with different stud arrangement. The initial stiffness for single-row-stud specimen was quite much smaller than normally-arranged-stud specimen, while that for per stud in each type of specimens showed similar results. With the same dimension of headed studs and shear pocket concrete, the stiffness of shear connectors was consistent in this study, irrespective of the arrangement of studs.

3.4 Ultimate strength

Table 3 also lists the ultimate load capacity per stud P_u , which was equal to the maximum shear strength divided by the number of connectors.

Generally, the ultimate strength did not show significant difference between specimens with different stud heights (from 100 mm to 200 mm) and slab thickness (from 200 mm to 300 mm). The maximum deviations for the variables of stud height and slab thickness were 1.81% and 5.57%, respectively. In this study, the specimens were failed in stud fracturing, with adjacent concrete crushing, cracking and spalling. In this case, the shear behaviour of interface between concrete slabs and steel beams depended on the properties of studs and surrounding concrete. For specimens with different stud height and slab thickness, both of the diameter of stud and the infilling concrete were identical. These results indicated that the anchor of 100 mm for studs with 22 mm diameter was sufficient, and the increasing of slab could not increase the bearing capacity of stud shear connectors.

According to the previously studies, it was well-known that the diameter of headed stud shear connectors was a vital parameter in the steel-concrete composite structures design. With the increasing of stud diameters, the ultimate strength of studs presented a major promotion. In this study, the shear capacity for specimens with the stud diameter of 25 mm was 1.55 times that of 19 mm stud, which also indicated that the cross-sectional area of the stud made a great contribution to the capacity of the shear connector.

The average shear capacity of a stud was 201.19 kN for specimens with C100 pocket concrete, and that for R125 concrete specimens was 210.72 kN. Compared with corresponding experimental results for C85 pocket concrete, these experimental results were much better. Compared with the C85 pocket concrete specimens, the specimens with higher infill material strength showed a smaller area of concrete crushing and no visible cracks adjacent the stud shanks. Furthermore, the restriction of stud deformation and constraints of stud from the higher strength concrete also made a full use of each stud even in

complex stress condition (Spremic *et al.* 2013). Additionally, the flexural, shear, and splitting resistance or the anchorage of stud were strengthened in high-strength concrete, especially in RPC materials (Alkaysi and El-Tawil 2017).

The addition of steel fiber in filling concrete has made a minor influence on the ultimate load of specimens. Though the compressive strength of concrete with both 1% and 2% steel fiber were almost equivalent to the C100 concrete, the paste of those was the same as the C85 concrete. It turned out that the strength of steel fiber concrete constituted with the compressive action of paste and the cracking resistance of fiber-bridge effect. This may one of the possible explanations for the effect of steel fiber in pocket concrete on the shear behaviour of steel-precast concrete slab composite structures.

The shear capacity per stud for single-row-connector specimens, however, was actually higher than that of normally arranged stud specimens. This may be caused by stress concentration, which was related to the space and number of adjacent studs (Xu *et al.* 2012). The rear studs sustained a lower shear stress than the front ones (Luo *et al.* 2016), which led to the greater plastic deformation in upper headed studs (Xue *et al.* 2012). This uneven shear force supporting of studs in group arrangement resulted in the local damage initiate earlier and develop faster (Xu *et al.* 2017b). As a result, the group arranged studs did not fail simultaneously and then strength reduction in per stud bear capacity occurred.

Minor deviations of the both ultimate strength and early shear-slip relationship (before peak load) were obtained between specimens with precast and cast-in-place methods. As listed in Table 3, the difference of mean shear capacity for per stud between 200/22-250-C85-0 (precast) and 200/22-250-MC85-0 (monolithic casting) was less than 1%. With the limitation of interface properties, casting methods had made a great influence in tests with normal strength concrete (49 MPa) (Wang *et al.* 2018a). However, the peak load of different casting method specimens was almost equivalent due to the same type of studs fracturing failure mode. The minor cracking and spalling of concrete near the stud root only showed slightly distinction in stiffness. Similar to the steel-precast UHPC slab tests (Wang *et al.* 2018a), the result in this study owed to the enhanced interface behaviour and the effective shear transfer between studs and concrete. Therefore, the post-casing methods may get an ideal effect closed to cast-in-place one, with the guarantee of sufficient interface shear bearing stress and concrete cracking resistance.

3.5 Ductility

Push-out specimens were considered to be ductile when the characteristic slip δ_{uk} was larger than 6 mm, as required in Eurocode 4 (Eurocode 2005). The characteristic resistance P_{RK} was taken as the ultimate shear strength P_u reduced by 10% (as depicted in Fig. 7). The slip capacity for a specimen δ_u was then considered as the maximum slip measured at the characteristic load P_{RK} . As for the characteristic slip δ_{uk} , was obtained as the minimum tested

Table 4 Typical design provisions for shear capacity of stud connector

Equation	Design Code	Theoretical model	Notation
(1)	Eurocode-4	$P_u = \frac{0.29\alpha d^2 \sqrt{f'_c E_c}}{\gamma_v} \leq \frac{0.8 f_u (\pi d^2 / 4)}{\gamma_v}$	H : the height of stud, mm; d : the diameter of stud, mm;
(2)	AASHTO LRFD	$P_u = 0.5 A_{sc} \sqrt{f'_c E_c} \leq A_{sc} f_u$	A_{sc} : the area of stud cross section, mm ² ; f_y : the yield strength of stud, MPa;
(3)	GB 50017	$P_u = 0.43 A_{sc} \sqrt{f'_c E_c} \leq 0.7 A_{sc} f_u \frac{f_u}{f_y}$	f_u : the ultimate tensile strength of stud, MPa; f'_c : the compressive strength of concrete, MPa;
(4)	JSCE	$P_u = \begin{cases} 10.32 d H \sqrt{f'_c} & (H/d < 5.5) \\ 56.4 d^2 \sqrt{f'_c} & (H/d > 5.5) \end{cases}$	E_c : the elastic module of concrete, MPa; α : aspect ratio factor, 1 in this study; γ_v : the partial factor, 1.25 for this study.

value of reduced by 10% (Euro code 2005). Both of the slip capacity and characteristic slip for all specimens are listed in Table 3.

Generally, more the height of the stud was large; the shear stud had a better ductility. All the specimens with stud height less than 150 mm could not meet the requirement of ductility. In current design code, stud aspect ratio (stud height/stud diameter) of larger than 4 was demanded for stud shank fracturing failure. Though the stud diameter of 22 mm was widely used in steel-concrete composite structure, thus the aspect ratio of 9.09 (200/22) was suggested for ductility purpose. Additionally, the ductility of tests with slab thickness of 200 mm and 250 mm was nearly identical, as presented in Table 3, but it obviously declined when the thickness increased to 300 mm. Hence, the thicker slab had a worse ductility. When choosing a suitable concrete slab thickness for steel-concrete composite bridge design, the equivalent shear capacity, increasing initial stiffness and materials, and the decreasing ductility and cracking should be combined simultaneously.

It can also be found that the ductility was improved with the increasing of stud diameter (from 19 mm to 22 mm), but it declined remarkable when the diameter increasing to 25 mm (68.10% lower than the 22 mm diameter one). This result indicated that the larger stud promoted the shear capacity and stiffness, with the losing of ductility. What's more, the stress concentration, poor welding quality and special manufacturing also limited the application of large headed stud (larger than 25 mm) in current practices (Wang *et al.* 2018a).

Meanwhile, compared with that with C85 concrete, the specimens with C100 concrete showed a 5.18% increase in ductility, but that of the specimens with R125 concrete decreased by 14.30%. The C100 concrete specimens provided appropriate range for the connectors to develop the deformation, causing the minor improvement of ductility. While the RPC specimens had recorded an acceptable mean characteristic slip δ_{uk} of 5.77 mm. There was no visible cracks but a small range of crushing around the stud, which might indicated that the most RPC materials surrounding the connectors were in the elastic (Wang *et al.* 2018a). This extra stiffness of RPC materials limited the deformation of studs to some extent. Therefore, it may also suggest that the headed stud shear connectors embedded in RPC concrete slab should be designed by elastic criterion to meet the ductility requirement (Kim *et al.* 2015).

Consequently, the ductility of the stud decreased gradually with the increasing steel fiber amount in pocket concrete, which can also be found from Table 3. Compared with the C100 specimens mentioned above, the addition of steel fiber in pocket concrete improved both the compressive strength and tensile resistance, which can also be confirmed via the smaller crushing area for steel fiber concrete specimens (Fig. 5). This resulted in the stiffer of both studs and concrete, which restricted the deformations of shear stud. Therefore, the addition of steel fiber would promote the ductility effectively, but without apparent improvement of bearing capacity or even declining the initial stiffness of specimens.

With identical studs and concrete materials, the ductility for single-row studs arrangement specimens (6.55 mm), controlling specimens (200/22-250-C85-0, 6.74 mm) and monolithic casting specimens (7.11 mm) were remarkable. As a reference, it can be found in the table, that monolithically cast specimens showed 5% more ductility than that of the precast specimens. Slight deviation for different stud arrangement tests showed that the stress concentration effect was acceptable and studs arranged in group might be an alternative choice at a narrow region or at steel-precast concrete slab composite structures. From the comparison between two casting methods studied in this paper, it can be confirmed that the precast steel-concrete composite structure can be adopted in practice engineering, with an acceptable ductility (6.74 mm) and minor decline of stiffness (4.93%) and shear capacity (0.98%).

4. Evaluation of test results

4.1 The existing design codes for stud shear capacity

Several equations for predicting the shear capacity of stud connectors have been developed based on the empirical data or finite element analysis results. To be more convective, only four typical design provisions as shown in Table 4 were considered, including Eurocode 4 (Eurocode 2005), AASHTO (AASHTO 2014), GB 50017 (GB 50017 2003), and JSCE (JSCE 2007). It should be noted that these theoretical models, except for Eq. (4) of JSCE, highly depended on the failure mode, such as stud fracture or concrete crushing. Moreover, these calculated results were

Table 5 Comparisons of experimental results and previous predictions

No.	Specimen	Experimental P_u (kN)	Eurocode 4		AASHTO LRFD		GB 50017		JSCE	
			$P_{eq.(1)}$ (kN)	$\frac{P_{eq.(1)}}{P_u}$	$P_{eq.(2)}$ (kN)	$\frac{P_{eq.(2)}}{P_u}$	$P_{eq.(3)}$ (kN)	$\frac{P_{eq.(3)}}{P_u}$	$P_{eq.(4)}$ (kN)	$\frac{P_{eq.(4)}}{P_u}$
1	200/19-250-C85-0a	162.33	85.41		133.45		128.40		190.74	
2	200/19-250-C85-0b	169.19	85.41	0.52	133.45	0.81	128.40	0.77	190.74	1.15
3	200/22-250-C85-0a	187.48	117.93		184.27		174.58		255.72	
4	200/22-250-C85-0b	195.10	117.93	0.62	184.27	0.96	174.58	0.91	255.72	1.34
5	200/25-250-C85-0a	271.31	144.23		225.37		215.88		330.22	
6	200/25-250-C85-0b	243.11	144.23	0.56	225.37	0.88	215.88	0.84	330.22	1.29
7	150/22-250-C85-0a	192.05	117.93		184.27		174.58		255.72	
8	150/22-250-C85-0b	187.48	117.93	0.62	184.27	0.97	174.58	0.92	255.72	1.35
9	100/22-250-C85-0a	188.24	117.93		184.27		174.58		212.69	
10	100/22-250-C85-0b	187.48	117.93	0.63	184.27	0.98	174.58	0.93	212.69	1.13
11	150/22-200-C85-0a	192.81	117.93		184.27		174.58		255.72	
12	150/22-200-C85-0b	182.14	117.93	0.63	184.27	0.98	174.58	0.93	255.72	1.37
13	150/22-300-C85-0a	185.95	117.93		184.27		174.58		255.72	
14	150/22-300-C85-0b	173.00	117.93	0.66	184.27	1.03	174.58	0.97	255.72	1.43
15	200/22-250-C100-0a	195.86	117.93		184.27		174.58		277.20	
16	200/22-250-C100-0b	206.53	117.93	0.59	184.27	0.92	174.58	0.87	277.20	1.38
17	200/22-250-R125-0a	212.63	117.93		184.27		174.58		305.54	
18	200/22-250-R125-0b	208.82	117.93	0.56	184.27	0.87	174.58	0.83	305.54	1.45
19	200/22-250-MC85-0a	192.81	117.93		184.27		174.58		255.72	
20	200/22-250-MC85-0b	193.57	117.93	0.61	184.27	0.95	174.58	0.90	255.72	1.32
21	200/22-250-C85-1a	195.86	117.93		184.27		174.58		275.44	
22	200/22-250-C85-1b	195.86	117.93	0.60	184.27	0.94	174.58	0.89	275.44	1.41
23	200/22-250-C85-2a	198.91	117.93		184.27		174.58		274.23	
24	200/22-250-C85-2b	195.86	117.93	0.60	184.27	0.93	174.58	0.88	274.23	1.39
25	S200/22-250-C85-0a	217.96	117.93		184.27		174.58		255.72	
26	S200/22-250-C85-0b	193.57	117.93	0.58	184.27	0.90	174.58	0.85	255.72	1.25
Mean			0.60		0.93		0.89		1.33	
Standard deviation			0.04		0.06		0.06		0.10	
Coefficient of variation			0.07		0.07		0.06		0.08	

always independent of the concrete compressive strength f_c' or elastic modulus E_c , when stud failure occurred. For the last one, JSCE (JSCE 2007) design code provided an equation with consideration of the stud geometry, concrete compressive strength and the aspect ratio H/d . The strength of head studs, however, has not been taken into account. In order to assess the applicability of these design specifications, as listed in Table 5, the calculated results were compared with the experimental ones in present study.

It can be seen from the results of comparison shown in Table 5, that Eqs. (1)-(3) gave a conservative prediction of stud shear capacity. Referring to the previous discussing, the concrete adjacent to the stud was often crushed even when the stud fractured. These underestimated predictions, thus, can be essentially explained by the lack of considering the interaction of concrete crushing and stud fracture.

Nevertheless, the JSCE design formula was quite adventurous predicting unsafe results. These results highlight the significance of taking account of the stud strength and the stress concentration effect.

4.2 Proposed equation and verification

As mentioned previously, the capacity of specimens presented in this study can rarely be predicted well by current design codes. Thus, a more applicable model was necessary for predicting the shear strength of interface between steel girder and high-strength precast concrete slab. According to the above discussion, both of the diameter of stud and the shear pocket concrete strength made an influence on the capacity of shear connectors. On the other hand, it has also been found that the shear capacity of studs

Table 6 Comparison of proposed equation with experimental results

Casting method	References	Predicted/Experimental [Eq. (5)]			Predicted/Experimental [Eq. (6)]		
		Mean	Standard deviation	Coefficient of variation	Mean	Standard deviation	Coefficient of variation
Precast	Present study	0.99	0.08	0.08	0.99	0.07	0.07
	Wang <i>et al.</i> (2018a)	1.13	0.07	0.06	1.01	0.06	0.06
	Xu <i>et al.</i> (2012)	1.03	0.06	0.06	1.03	0.06	0.06
	Present study	0.98	0	0	0.98	0	0
	Wang <i>et al.</i> (2018a)	1.04	0.05	0.05	1.00	0.06	0.06
	Cao <i>et al.</i> (2017)	1.11	0.04	0.04	0.97	0.04	0.04
Cast-in-place	Kim <i>et al.</i> (2015)	1.24	0.24	0.20	0.95	0.05	0.05
	Liu and Alkhatib (2013)	0.88	0.09	0.10	0.92	0.09	0.10
	Xu <i>et al.</i> (2012)	0.78	0.05	0.06	0.89	0.05	0.06
	Lee <i>et al.</i> (2005)	0.91	0.11	0.12	0.98	0.08	0.09
	Lam and El-Lobody (2005)	0.84	0.03	0.04	0.98	0.13	0.14
	Shim <i>et al.</i> (2004)	1.01	0.14	0.14	1.10	0.08	0.08
	Loh <i>et al.</i> (2004)	0.74	0	0	1.02	0	0
	Gattesco and Giuriani (1996)	0.70	0	0	0.97	0	0
	Li and Cederwall (1996)	0.86	0.09	0.10	0.97	0.03	0.03

was affected by the material properties of shear connectors. Based on the equations listed in Table 4, the proposed one incorporated a component of the area of stud cross section (A_{sc}), the ultimate tensile strength of stud (f_u) and the compressive strength of concrete (f_c). Specially, the form of $\sqrt{f_c}$ was used due to its acceptable prediction and simple form, but also its widely adoption in current design codes listed above. Similar to the proposals of several authors, multiple regression analysis was performed to propose an equation adjusted to the results presented in this study. With the analysis on the experimental data, the proposed equation was then expressed as

$$P_u = 0.11A_{sc}f_u\sqrt{f_c} \quad (5)$$

Combined with the properties of both headed stud and concrete, Eq. (5) agreed well with the test results in this study, as shown in Table 6. The mean value and standard deviation between predicted and experimental value by Eq. (5) were 0.99 and 0.08 for precast slab case, respectively. While for cast-in-place condition, the relation and standard deviation between them were 0.98 and 0.00, respectively. Specially, the results in this paper showed that no apparent deviation for the shear strength between different casting methods, due to the sufficient compressive strength of surrounding concrete. This equation, thus, can be used for predicting both precast and cast-in-place cases. On the other hand, all the tests in this study failed in stud fracture, with slight crushing of concrete adjacent the stud root, which has limited the Eq. (5) to only the stud fracture situation.

4.3 Validation and correction of the proposed equation

In order to assess the applicability of Eq. (5), the related

experimental results obtained by Wang *et al.* (2018a), Cao *et al.* (2017), Kim *et al.* (2015), Liu and Alkhatib (2013), Xu *et al.* (2012), Lee *et al.* (2005), Lam and El-Lobody (2005), Shim *et al.* (2004), Loh *et al.* (2004), Gattesco and Giuriani (1996), Li and Cederwall (1996) were considered. These results contained the casting method of both precast (PC) and cast-in-place (CIP) cases, with the stud diameter ranging from 13 mm to 30 mm and the concrete strength varying from 26 MPa to 200 MPa. The comparison of experimental and predicted results in Table 6 showed that the mean of predicted/experimental results ranged from 1.03 to 1.13 for precast slab and 0.70 to 1.24 for cast-in-place slab. This conclusion can also be drawn from Fig. 8(a). Interestingly, the higher concrete strength for Wang *et al.* (2018a) (125.4 MPa) and Kim *et al.* (2015) (200 MPa) may be reason for the overestimated prediction. On the contrary, the relatively lower concrete strength for Lee *et al.* (2005) (40 MPa), Kim *et al.* (2015) (35 MPa), Li and Cederwall (1996) (30.77 MPa) and Loh *et al.* (2004) (26.2 MPa) provided an underestimated results.

In the case of high-strength concrete, the confining effect on stud has been limited when the strength reached a constant level, which meant that the influence of concrete strength would be neglected at a certain value. Similarly, the tensile strength and deformation resistance for concrete has been neglected in Eq. (5), while those were very important in lower concrete strength condition. Based on the analysis of both present and previous results, it was suggested that the values of 50 MPa and 100 MPa for concrete strength were a suitable boundary for the proposed model. Additionally, it was also suggested that the multiplier/coefficient α of 1.15 should be considered for single-row arrangement case, resulted from the non-simultaneous failure of shear connectors at different rows (heights) (Xu *et al.* 2012). As a result, the corrected

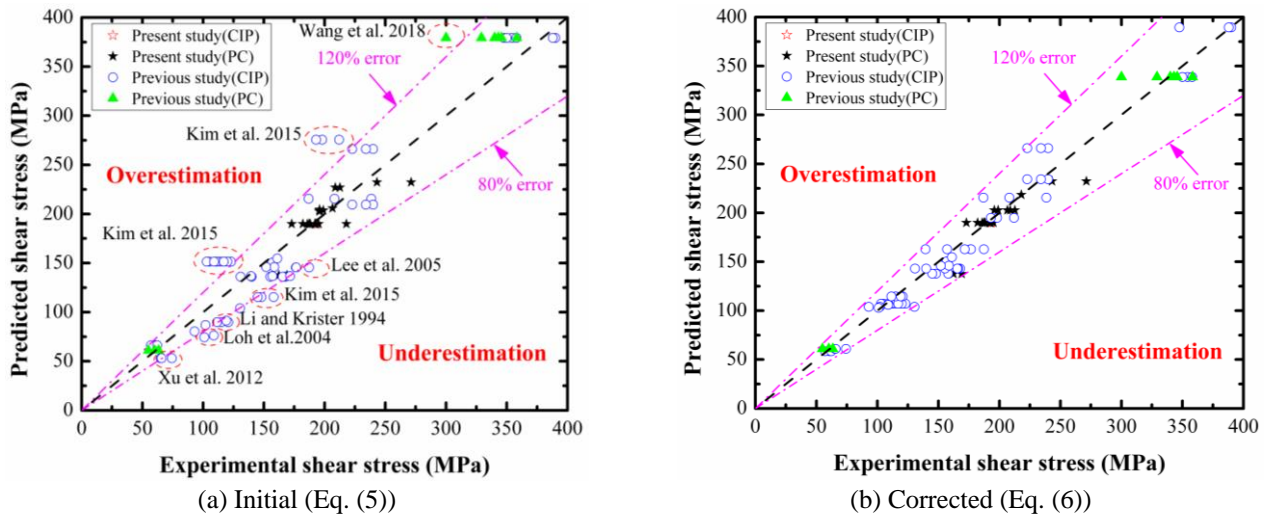


Fig. 8 Evaluation of proposed shear resistance equation

equation for shear capacity between steel beam and precast slab was proposed as

$$P_u = \begin{cases} 0.78\alpha_{sc} f_u & f'_c \leq 50 \text{ MPa} \\ 0.11\alpha_{sc} f_u \sqrt{f'_c} & 50 \text{ MPa} \leq f'_c \leq 100 \text{ MPa} \\ 1.1\alpha_{sc} f_u & f'_c \geq 100 \text{ MPa} \end{cases} \quad (6)$$

With the correction of proposed equation, pretty good agreements between the experimental and calculated results can be found from both Table 6 and Fig. 8. The means of predicted/experimental results for all the comparison were varied from 0.89 to 1.10. However, the authors suggest that more experimental results of interface shear resistance between steel beam and precast concrete slab are needed to verify the applicability of the proposed empirical equations. And the range of application should also be expanded to the concrete slab splitting failure or other situations.

5. Conclusions

Twenty-six push-put tests were conducted in this study to investigate the shear behavior of the connectors between precast high-strength concrete slab and steel beams. The influence of stud height, stud diameter, deck thickness, and cast-in-place concrete strength, steel fiber volume, casting method and the arrangement of stud on failure modes, initial stiffness, ultimate strength and ductility of specimens have been explored. Based on the results of this research, the main conclusions are as follows.

- Most of the specimens exhibited similar 4-stage load-slip relationships, which can be relative to the shear failure modes that combined both stud fracture and concrete crushing.
- Increase of stud diameter, infilling concrete strength and steel fiber volume made specimens stiffer. On the other hand, the initial stiffness of shear connector was slightly affected by the precast concrete deck thickness and casting method, but insensitive to the height of stud. Compared with normal arrangement stud specimens, the

stiffness for single-row specimens were apparent smaller, but that for per stud showed similar results for both type of specimens.

- The capacity of shear connectors was closely related to both the stud diameter and shear pocket concrete strength, slightly affected by the steel fiber volume and stud arrangement, but insensitive to the stud height, slab thickness and casting method. With the guarantee of sufficient interface shear bearing stress and concrete cracking resistance, this study suggested that the post-casting methods may get an ideal effect closed to cast-in-place one.
- Specimens with higher stud, thinner concrete slab and less steel fiber in shear pocket concrete showed better ductility. Additionally, monolithic casting specimens presented good ductility while the single-row-stud specimens gave a poor result. The ductility of specimens increased with the increasing of stud diameter and the cast-in-place concrete strength, but decreased with the continued increasing.
- The formulas in Euro 4, AASHTO and GB 50017 showed conservative prediction while that in JSCE overestimated the shear capacity. A more accurate model based on multiple regression analysis of test results of authors was proposed and verified by other experimental results. Considered with the stud arrangement and the properties of both stud and concrete, it can be used to predict the interface shear capacity well for specimens with wide ranges of the stud diameters (from 13 mm to 30 mm) and the concrete strength (from 26 MPa to 200 MPa).

Acknowledgments

The research presented was funded by National Natural Science Foundation of China (51778150), Science and Technology Planning Project of Guangzhou city (201804010422) in China, and Natural Science Foundation of Guangdong Province, China (2016A030313699). The

authors gratefully acknowledge their generous supports and declare that they have no conflict of interests.

References

- AASHTO (2014), AASHTO LRFD bridge design specifications; (7th Ed.), American Association of State Highway and Transportation Officials, Washington D. C., USA.
- Alkaysi, M. and El-Tawil, S. (2017), "Factors affecting bond development between Ultra High Performance Concrete (UHPC) and steel bar reinforcement", *Constr. Build. Mater.*, **144**, 412-422. <https://doi.org/10.1016/j.conbuildmat.2017.03.091>.
- An, L. and Cederwall, K. (1996), "Push-out tests on studs in high strength and normal strength concrete", *J. Constr. Steel Res.*, **36**(1), 15-29. [https://doi.org/10.1016/0143-974X\(94\)00036-H](https://doi.org/10.1016/0143-974X(94)00036-H).
- ASTM (2011), *C496/C496M-11*, Standard test method for splitting tensile strength of cylindrical concrete specimens, ASTM International; West Conshohocken, PA, USA.
- ASTM (2014), *C469/C469M-14*, Standard test method for static modulus of elasticity and Poisson's ratio of concrete in compression, ASTM International; West Conshohocken, PA, USA.
- ASTM (2015), *C1231/C1231M-15*, Standard practice for use of unbond caps in determination of compressive strength of hardened cylindrical concrete specimens, ASTM International; West Conshohocken, PA, USA.
- Cao, J.H., Shao, X.D., Deng, L. and Gan, Y.D. (2017), "Static and fatigue behavior of short-headed studs embedded in a thin ultrahigh-performance concrete layer", *J. Bridge Eng.*, **22**(5), 04017005. [https://doi.org/10.1061/\(ASCE\)BE.1943-5592.0001031](https://doi.org/10.1061/(ASCE)BE.1943-5592.0001031).
- Chu, T.H.V., Bui, D.V., Le, V.P.N., Kim, I.T., Ahn, J.H. and Dao, D.K. (2016), "Shear resistance behaviors of a newly puzzle shape of crested rib shear connector: An experimental study", *Steel Compos. Struct.*, **21**(5), 1157-1182. <https://doi.org/10.12989/scs.2016.21.5.1157>.
- Classen, M. and Hegger, J. (2018), "Shear-slip behaviour and ductility of composite dowel connectors with pry-out failure", *Eng. Struct.*, **150**, 428-37. <https://doi.org/10.1016/j.engstruct.2017.07.065>.
- Eurocode 4 (2005), Design of composite steel and concrete structure: Part 2: General rules for bridge, European Committee for Standardization (CEN); Brussels, Belgium.
- Fanaie, N., Esfahani, F.G and Soroushnia, S. (2015), "Analytical study of composite beams with different arrangements of channel shear connectors", *Steel Compos. Struct.*, **19**(2), 485-501. <https://doi.org/10.12989/scs.2015.19.2.485>.
- Fang, Z.C., Jiang, H.B. Liu, A.R., Feng, J.H. and Chen, Y. (2018), "Horizontal shear behaviors of normal weight and lightweight concrete composite T-beams", *Int. J. Concr. Struct. M.*, **12**(1), 15-24. <https://doi.org/10.1186/s40069-018-0274-3>.
- Gattesco, N. and Giuriani, E. (1996), "Experimental study on stud shear connectors subjected to cyclic loading", *J. Constr. Steel Res.*, **38**(1), 1-21. [https://doi.org/10.1016/0143-974X\(96\)00007-7](https://doi.org/10.1016/0143-974X(96)00007-7).
- GB 50017 (2003), Code for design of steel structures, China Planning Press; Beijing, PR China minister of China. GB 50017-2003: China Planning Press, 2003.
- Han, Q.H., Wang, Y.H., Xu, J. and Xing, Y. (2015), "Static behavior of stud shear connectors in elastic concrete-steel composite beams", *J. Constr. Steel Res.*, **113**, 115-126. <https://doi.org/10.1016/j.jcsr.2015.06.006>.
- JSCE (2007), Standard specification for steel and composite structures (design edition), Committee of steel structure; Japan.
- Ju, X.C. and Zeng, Z.B. (2015), "Study on uplift performance of stud connector in steel-concrete composite structures", *Steel Compos. Struct.*, **18**(5), 1279-1290. <https://doi.org/10.12989/scs.2015.18.5.1279>.
- Kim, J.S., Kwark, J., Joh, C., Yoo, S.W. and Lee, K.C. (2015), "Headed stud shear connector for thin ultrahigh-performance concrete bridge deck", *J. Constr. Steel Res.*, **108**, 23-30. <https://doi.org/10.1016/j.jcsr.2015.02.001>.
- Kim, S.H., Choi, K.T., Park, S.J., Park, S.M. and Jung, C.Y. (2013), "Experimental shear resistance evaluation of Y-Type perfobond rib shear connector", *J. Constr. Steel Res.*, **82**, 1-18. <https://doi.org/10.1016/j.jcsr.2012.12.001>.
- Kim, S.H., Jung, C.Y. and Ahn, J.H. (2011), "Ultimate strength of composite structure with different degrees of shear connection", *Steel Compos. Struct.*, **11**(5), 375-390. <https://doi.org/10.12989/scs.2011.11.5.375>.
- Kim, K.S., Han, O., Gombosuren, M. and Kim, S.H. (2019), "Numerical simulation of Y-type perfobond rib shear connectors using finite element analysis", *Steel Compos. Struct.*, **31**(1), 53-67. <https://doi.org/10.12989/scs.2019.31.1.053>.
- Lam, D. (2008), "Capacities of headed stud shear connectors in composite steel beams with precast hollowcore slabs", *J. Constr. Steel Res.*, **63**(9), 1160-1174. <https://doi.org/10.1016/j.jcsr.2006.11.012>.
- Lam, D. and El-Lobody, E. (2005), "Behavior of headed stud shear connectors in composite beam", *J. Struct. Eng.*, **131**(1), 96-107. [https://doi.org/10.1061/\(ASCE\)0733-9445\(2005\)131:1\(96\)](https://doi.org/10.1061/(ASCE)0733-9445(2005)131:1(96)).
- Lee, P.G., Shim, C.S. and Chang, S.P. (2005), "Static and fatigue behavior of large stud shear connectors for steel-concrete composite bridges", *J. Constr. Steel Res.*, **61**, 1270-1285. <https://doi.org/10.1016/j.jcsr.2005.01.007>.
- Lee, Y.H., Kim, M.S., Kim, H. and Kim, D.J. (2014), "Shear resistance of stud connectors in high strength concrete", *Steel Compos. Struct.*, **52**(4), 647-661. <https://doi.org/10.12989/sem.2014.52.4.647>.
- Liu, X.P., Bradford, M.A. Dist. and Lee, M.S.S. (2015), "Behavior of high-strength friction-grip bolted shear connectors in sustainable composite beams", *J. Bridge Eng.*, **141**(6), 04014149. [https://doi.org/10.1061/\(ASCE\)ST.1943-541X.0001090](https://doi.org/10.1061/(ASCE)ST.1943-541X.0001090).
- Liu, Y., and Alkhatib, A. (2013), "Experimental study of static behaviour of stud shear connectors", *Can. J. Civil Eng.*, **40**(9), 909-916. <https://doi.org/10.1139/cjce-2012-0489>.
- Loh, H., Uy, B. and Bradford, M. (2004), "The effects of partial shear connection in the hogging moment regions of composite beams, Part I—Experimental study", *J. Constr. Steel Res.*, **60**(6), 897-919. <https://doi.org/10.1016/j.jcsr.2003.10.007>.
- Luo, Y.B., Hoki, K., Hayashi, K. and Nakashima, M. (2016), "Behavior and strength of headed stud-SFRCC shear connection. II: Strength evaluation", *J. Struct. Eng.*, **142**, 04015113. [https://doi.org/10.1061/\(ASCE\)ST.1943-541X.0001372](https://doi.org/10.1061/(ASCE)ST.1943-541X.0001372).
- Machacek, J. and Studnicka, J. (2002), "Perforated shear connectors", *Steel Compos. Struct.*, **2**(1), 51-66. <https://doi.org/10.12989/scs.2002.2.1.051>.
- Mazoz, A., Benanane, A. and Titoum, M. (2013), "Push-out tests on a new shear connector of I-shape", *Int. J. Steel Struct.*, **13**(3), 519-28. <https://doi.org/10.1007/s13296-013-3011-4>.
- Milosavljevic, B., Milicevic, I., Pavlovic, M. and Spremic, M. (2018), "Static behaviour of bolted shear connectors with mechanical coupler embedded in concrete", *Steel Compos. Struct.*, **29**(2), 257-272. <https://doi.org/10.12989/scs.2018.29.2.257>.
- Noel, M., Wahab, N. and Soudki, K. (2016), "Experimental investigation of connection details for precast deck panels on concrete girders in composite deck construction", *Eng. Struct.*, **106**, 15-24. <https://doi.org/10.1016/j.engstruct.2015.10.002>.
- Paknahad, M., Shariati, M., Sedghi, Y., Bazzaz, M. and Khorami, M. (2018), "Shear capacity equation for channel shear connectors in steel-concrete composite beams", *Steel Compos. Struct.*, **28**(4), 483-494. <https://doi.org/10.12989/scs.2018.28.4.483>.
- Pavlović, M., Marković, Z., Veljković, M. and Buđevac, D. (2013), "Bolted shear connectors vs. headed studs behaviour in push-out tests", *J. Constr. Steel Res.*, **88**, 134-149. <https://doi.org/10.1016/j.jcsr.2013.05.003>.
- Qi, J.N., Wang, J.Q., Li, M. and Chen, L.L. (2017), "Shear capacity of

- stud shear connectors with initial damage: Experiment, FEM model and theoretical formulation”, *Steel Compos. Struct.*, **25**(1), 79-92. <https://doi.org/10.12989/scs.2017.25.1.079>.
- Shariati, M., Sulong, N.H.R., Suhatri, M., Shariati, A., Khanouki, M.M.A. and Sinaei, H. (2012), “Behaviour of C-shaped angle shear connectors under monotonic and fully reversed cyclic loading: an experimental study”, *Mater. Design*, **41**, 67-73. <https://doi.org/10.1016/j.matdes.2012.04.039>.
- Shim, C.S., Lee, P.G. and Chang, S.P. (2001), “Design of shear connection in composite steel and concrete bridges with precast decks”, *J. Constr. Steel Res.*, **57**(3), 203-219. [https://doi.org/10.1016/S0143-974X\(00\)00018-3](https://doi.org/10.1016/S0143-974X(00)00018-3).
- Shim, C.S., Lee, P.G. and Yoon, T.Y. (2004), “Static behavior of large stud shear connectors”, *Eng. Struct.*, **26**(12), 1853-1860. <https://doi.org/10.1016/j.engstruct.2004.07.011>.
- Spremic, M., Markovic, Z., Veljkovic, M., and Budjevac, D (2013), “Push-out experiments of headed shear studs in group arrangement”, *Adv. Steel Constr.*, **9**, 139-60. <https://doi.org/10.18057/IJASC.2013.9.2.4>
- Su, Q.T., Yang, G.T. and Bradford, M.A. (2014), “Static behaviour of multi-row stud shear connectors in high-strength concrete”, *Steel Compos. Struct.*, **17**(6), 967-980. <https://doi.org/10.12989/scs.2014.17.6.967>.
- Wang, J.Q., Xu Q.Z., Yao, Y.M., Qi, J.N. and Xiu, H.L. (2018a), “Static behavior of grouped large headed stud-UHPC shear connectors in composite structures”, *Compos. Struct.*, **206**, 202-14. <https://doi.org/10.1016/j.compstruct.2018.08.038>.
- Wang, X.W., Zhu, B., Cui, S.A. and Lui, E.M. (2018b), “Experimental Research on PBL Connectors Considering the Effects of Concrete Stress State and Other Connection Parameters”, *J. Bridge Eng.*, **23**(1), 04017125. [https://doi.org/10.1061/\(ASCE\)BE.1943-5592.0001158](https://doi.org/10.1061/(ASCE)BE.1943-5592.0001158).
- Xu, C. and Sugiura, K. (2013), “FEM analysis on failure development of group studs shear connector under effects of concrete strength and stud dimension”, *Eng. Fail. Anal.*, **35**, 343-354. <https://doi.org/10.1016/j.engfailanal.2013.02.023>.
- Xu, C. and Sugiura, K. (2014), “Analytical investigation on failure development of group studs shear connector in push-out specimen under biaxial load action”, *Eng. Fail. Anal.*, **37**, 75-85. <https://doi.org/10.1016/j.engfailanal.2013.11.010>.
- Xu, C., Su, Q.T. and Masuya, H. (2017a), “Static and fatigue performance of stud shear connector in steel fiber reinforced concrete”, *Steel Compos. Struct.*, **24**(4), 467-479. <https://doi.org/10.12989/scs.2017.24.4.467>.
- Xu, C., Su, Q.T. and Sugiura, K. (2017b), “Mechanism study on the low cycle fatigue behavior of group studs shear connectors in steel-concrete composite bridges”, *J. Constr. Steel Res.*, **138**, 196-207. <https://doi.org/10.1016/j.jcsr.2017.07.006>.
- Xu, C., Sugiura, K., Wu, C. and Su, Q.T. (2012), “Parametrical static analysis on group studs with typical push-out tests”, *J. Constr. Steel Res.*, **72**, 84-96. <https://doi.org/10.1016/j.jcsr.2011.10.029>.
- Xu, X.Q., Liu, Y.Q. and He, J. (2014), “Study on mechanical behavior of rubber-sleeved studs for steel and concrete composite structures”, *Constr. Build. Mater.*, **53**, 533-546. <https://doi.org/10.1016/j.conbuildmat.2013.12.011>.
- Xue, D.Y., Liu, Y.Q., Yu, Z. and He, J. (2012), “Static behavior of multi-stud shear connectors for steel-concrete composite bridge”, *J. Constr. Steel Res.*, **74**, 1-7. <https://doi.org/10.1016/j.jcsr.2011.09.017>.
- Yang, F., Liu, Y.Q., Jiang, Z.B. and Xin, H.H. (2018), “Shear performance of a novel demountable steel-concrete bolted connector under static push-out tests”, *Eng. Struct.*, **160**, 133-146. <https://doi.org/10.1016/j.engstruct.2018.01.005>.
- Zheng, S.J., Liu, Y.Q., Yoda, T. and Lin, W.W. (2016a), “Parametric study on shear capacity of circular-hole and long-hole perfobond shear connector”, *J. Constr. Steel Res.*, **117**, 64-80. <https://doi.org/10.1016/j.jcsr.2015.09.012>.
- Zheng, S.J., Liu, Y.Q., Yoda, T. and Lin, W.W. (2016b), “Shear behavior and analytical model of perfobond connectors”, *Steel Compos. Struct.*, **20**(1), 71-89. <https://doi.org/10.12989/scs.2016.20.1.071>.
- Zhu, Z.H., Zhang, L., Bai, Y., Ding, F.X., Liu, J. and Zhou, Z. (2016), “Mechanical performance of shear studs and application in steel-concrete composite beams”, *J. Cent. South Univ.*, **23**(10), 2676-2687. <https://doi.org/10.1007/s11771-016-3329-0>.

CC